Arabian Journal of Chemistry (2020) 13, 3790–3800

King Saud University

Arabian Journal of Chemistry

www.ksu.edu.sa
www.sciencedirect.com

ORIGINAL ARTICLE

ZnO-Bi_2O_3/graphitic carbon nitride photocatalytic system with H_2O_2-assisted enhanced degradation of Indigo carmine under visible light

Bui The Huy [a,b], Da Seul Paeng [a], Chu Thi Bich Thao [a], Nguyen Thi Kim Phuong [c,*], Yong-Ill Lee [a,*]

[a] *Department of Chemistry, Changwon National University, Changwon 51140, Republic of Korea*
[b] *Institute for Research and Development, Duy Tan University, 03 Quang Trung, Da Nang, Viet Nam*
[c] *HoChiMinh City Institute of Resources Geography, Vietnam Academy of Science and Technology, 01 Mac Dinh Chi, District 1, Ho Chi Minh City, Viet Nam*

Received 20 November 2018; accepted 10 January 2019
Available online 23 January 2019

KEYWORDS

Indigo carmine;
Hydroxyl radicals;
Photocatalyst;
Degradation;
Mineralization

Abstract Indigo carmine in aqueous solution was effectively degraded using ZnO-Bi_2O_3/Graphitic Carbon Nitride heterojunction structure by visible light/H_2O_2 system. The mechanism of photocatalytic degradation of Indigo carmine shows the responsible species for the degradation of Indigo carmine in the ZnO-Bi_2O_3-xC_3N_4/H_2O_2/visible light system (x = 0, 1, 2, and 3) is the hydroxyl radicals which were generated from the reaction of e^- and h^+ with H_2O_2. Under optimal conditions, ZnO-Bi_2O_3-$2C_3N_4$/H_2O_2/Vis system degraded more than 93% of Indigo carmine in 180 min. Besides, the kinetic of the photocatalytic process was detailed. These results demonstrate that the ZnO-Bi_2O_3-$2C_3N_4$/H_2O_2/visible light system may become a promising approach to achieve efficient environmental remediation as an environmentally friendly oxidant.

1. Introduction

Environmental pollution related to the dye residues from textile industry is currently an urgent issue. The most widely used dye in the textile industry is Indigo carmine (Indigo-5, 5′-disulfonic acid disodium salt). Besides using it as a textile dye, it can also be used as an additive in pharmaceuticals for medical diagnosis purposes (Barka et al., 2008). The high toxicity of indigo carmine can cause tumors, hypertension, disturbance of reproductive and nervous systems, well documented in the literature (Barka et al., 2008). Nowadays, the removal of harmful organic pollutants through advanced oxidation

* Corresponding authors.
E-mail addresses: nguyenthikimp@yahoo.ca (N.T. Kim Phuong), yilee@changwon.ac.kr (Y.-I. Lee).
Peer review under responsibility of King Saud University.

Production and hosting by Elsevier

https://doi.org/10.1016/j.arabjc.2019.01.003
1878-5352

processes (AOPs) including Fenton oxidation, photocatalytic oxidation and electrolytic oxidation are attracting an increasing attention, because these processes can create powerful oxidizing species such as electrons, holes, $OH^{\bullet}$ radicals, and $O_2^{\bullet-}$ radicals (Oturan et al., 2000, Irmak et al., 2006, Wang et al., 2009a, Wang et al., 2009b, Yap et al., 2011, Virkutyte and Varma, 2014). Photo-Fenton oxidation is one of the most promising AOPs. The main advantage of this oxidation process is the efficient production of highly active hydroxyl ($OH^{\bullet}$) radicals which will attack organic pollutants found in wastewater (Gemeay et al., 2003).

Hydrogen peroxide (H_2O_2) is a moderately oxidizing agent for a variety of organic compounds. However, H_2O_2 decomposes slowly at room temperature; therefore, the oxidizing capability of H_2O_2 is often enhanced with catalysts, UV-light, ultrasound, or heat, to generate reactive oxygen species to oxidize organic compounds (Centi et al., 2000, Gemeay et al., 2003). Until now, limited studies have been carried out using visible light-H_2O_2 system for degradatingorganic compounds.

The growing awareness of photocatalytic semiconductor has led to an increasing demand for environmental treatment and energy production due to formed electron-hole pairs, followed by the separation of charge pairs (Wang et al., 2015, Xu et al., 2015, Patnaik et al., 2018b). Among various semiconductors, the oxides of Mo, Zn, Bi, Ti, and Sn elements are more suitable for photocatalytic processes (Xu et al., 2015, Patnaik et al., 2018c). However, their photocatalytic efficiencies were very low because of the wide band gaps and relatively high electron-hole recombination rates. In order to improve photocatalytic efficiency, the heterostructural semiconductors have been utilized as potential candidates (Cao et al., 2012, Cui et al., 2014, Jiang et al., 2014, Xu et al., 2015, Zhang et al., 2015, Yan et al., 2016, Patnaik et al., 2017). The photocatalytic activities of heterostructural semiconductors is much better than those of single component semiconductors because the probabilities of light absorption, charge transfer, and photogenerated electron-hole pair separation are improved through the junctions at the interfaces (Hu et al., 2014, Yan et al., 2016). It has been revealed that the heterojunctions of graphitic carbon nitride (C_3N_4) with composite catalysts enhanced the photocatalytic efficiency due to medium band gap, thermal and chemical stability of C_3N_4 (Chai et al., 2012, Ding et al., 2013, Fu et al., 2013, Chunyan et al., 2016, Shi et al., 2016, Ruiru et al., 2017, Cui et al., 2018, Dong et al., 2018, Li et al., 2018a, Li et al., 2018b, Nayak and Parida, 2018, Patnaik et al., 2018a, Chen et al., 2019).

The mixed metal oxides obtained by heating the double layer hydroxide (LDH) have been adapted for improving catalytic capability to degrade several pollutant compounds. (Mendoza-Damián et al., 2013, Xiang et al., 2013, Mohapatra and Parida, 2014, Kim Phuong et al., 2016, Bui et al., 2017). In our previous report, the LDH based on the hybrid composite of zinc bismuth oxide and graphitic carbon nitride (ZnO-Bi_2O_3-xC_3N_4) exhibited high photocatalytic efficiency for the mineralization of Rhodamine B (Bui et al., 2017). We suggested that the degradation mechanism of Rhodamine B by ZnO-Bi_2O_3-xC_3N_4 under visible light is mainly due to the photoinduced hole. It is well known that the efficiency of dyes degradation in aqueous solution depends on the synergistic effect between the dyes and catalysts, and other influencing factors such as pH, free radicals, energy sources, and the structure of dye. The degradation mechanisms of different dyes are largely different because of the structural difference of dyes. The ZnO-Bi_2O_3-xC_3N_4 material with the assistance of H_2O_2/visible light is anticipated to exhibit an excellent catalytic activity for degradating Indigo carmine which is a high toxic industrial dye. In this work, we present the studies on the efficacy, mechanism, and kinetics of H_2O_2-assisted degradation of Indigo carmine by ZnO-Bi_2O_3-xC_3N_4 phtocatalytic system under visible light.

2. Experimental

The synthesized procedure and studies on morphology of ZnO-Bi_2O_3-xC_3N_4 material were followed in our previous report (Bui et al., 2017) and presented in Supporting information. The photocatalytic activity of the materials was estimated based on degradation reaction of Indigo carmine under visible light using a Xenon lamp 150 W (Model No. LS 150 SN 332 ABET Technologies, USA). To maintain a fixed temperature of the reaction mixture, the water in the mantle of the reactor was circulated. In all photocatalytic experiments, 50 mg of catalyst was added in a 100 mL of Indigo carmine solution (50 mg/L) at pH ~ 7.0. The suspension was exposed under Xenon light lamp after 60 min in a dark room to set up the adsorption-desorption equilibrium between the Indigo carmine and the catalyst. At different time intervals, the amount of Indigo carmine in solution was determined by the UV–Vis absorption measurement at a wavelength of 612 nm by using a Thermo Evolution 201 UV–Visible spectrophotometer (U.S.). The reactions were performed in triplicate. Doubly distilled water was used throughout this study. For the reaction in H_2O_2-Vis light system, 2.14 mmol/L H_2O_2 was added immediately to a 100 mL solution (50 mg/L of Indigo carmine and 50 mg of the catalysts) at pH 7.0 and then illuminated with visible light.

The effects of the initial catalyst amount, initial pH of the solution, and H_2O_2 concentrations on the degradation of Indigo carmine in the catalyst-H_2O_2-Vis system were investigated. The radical trapping study was performed by adding two scavengers to the solution: (i) ethanol (C_2H_5OH, 2.0 mmol/L) as an $OH^{\bullet}$ radical scavenger and (ii) ascorbic acid ($C_6H_8O_6$, 2.0 mmol/L) as a superoxide anion radical scavenger.

3. Results and discussion

The synthetic procedure and characterizations of ZnO-Bi_2O_3-xC_3N_4 samples were studied and presented in Supporting information, as shown in Figs. S1 and S2.

3.1. Synergic effect between the catalysts (ZnO-Bi_2O_3-xC_3N_4, $x = 0, 1, 2, 3$), visible light (Vis), and H_2O_2 on the degradation of Indigo carmine

The photocatalytic activities of the ZnO-Bi_2O_3-xC_3N_4 were assessed in a series of experiments based on Indigo carmine degradation. As shown in Fig. 1A, the self-decomposition of Indigo carmine can be ignored due to the negligible amount (~6.4%) of Indigo carmine degradation over the 180 min visible light irradiation. As a control, the photocatalytic ability of ZnO-Bi_2O_3, and pristine C_3N_4 were also evaluated. Over the 180 min under visible light irradiation, ZnO-Bi_2O_3, pristine

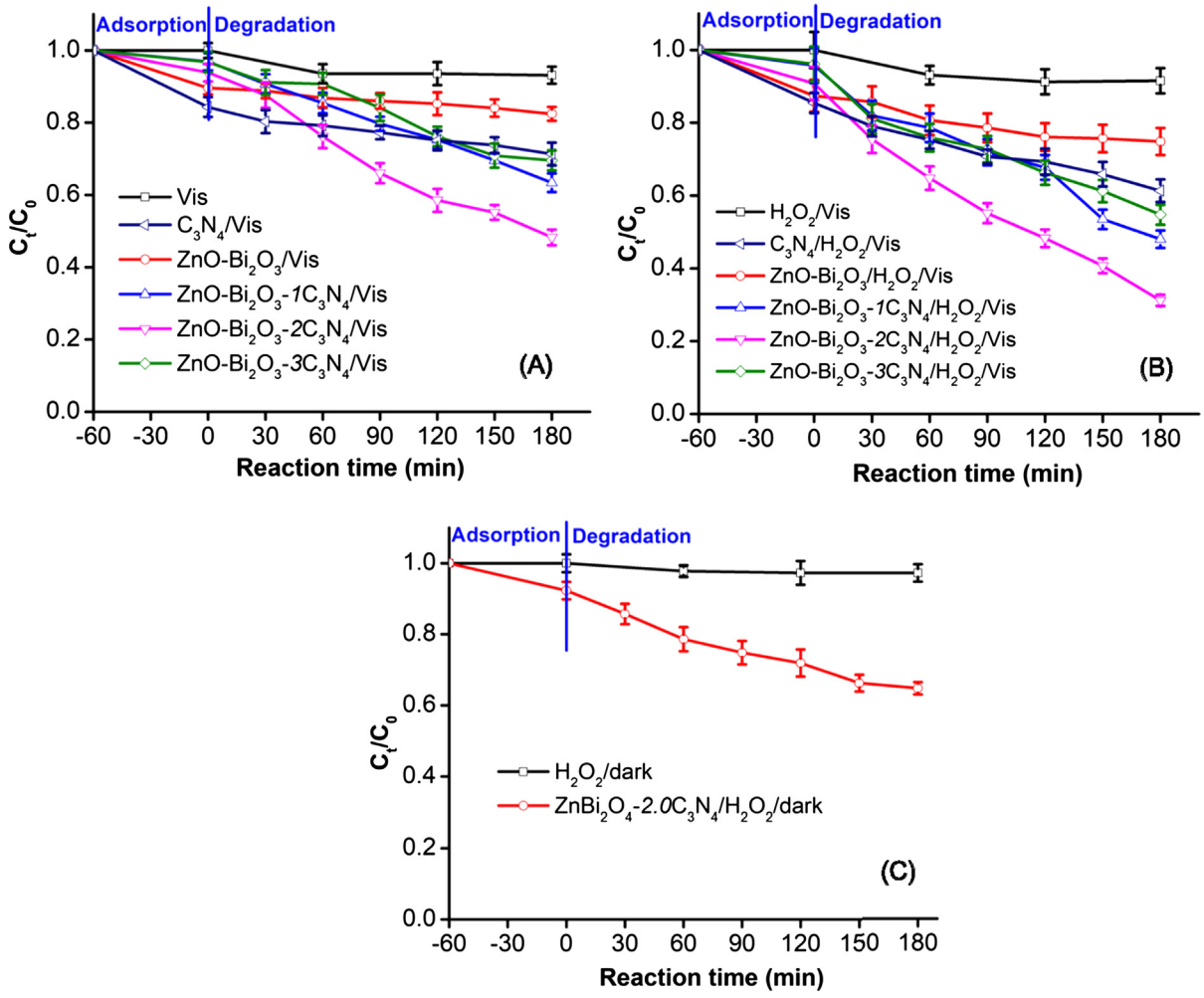

Fig. 1 Photocatalytic activities of (A) ZnO-Bi_2O_3-xC_3N_4/Vis system; (B) ZnO-Bi_2O_3-xC_3N_4/H_2O_2/Vis system, and (C) ZnO-Bi_2O_3-xC_3N_4 /H_2O_2/dark system for Indigo carmine degradation.

C_3N_4 samples degraded gradually approximately 17.6%, and 26.7% of the Indigo carmine, respectively. This indicated that either pristine ZnO-Bi_2O_3 or pristine C_3N_4 possessed relatively weak photocatalytic ability under visible light. Whereas the heterostructural catalyst, ZnO-Bi_2O_3-xC_3N_4 exhibited much better photocatalytic performance than ZnO-Bi_2O_3 by the incorporation of g-C_3N_4 into the ZnO-Bi_2O_3 structure. ZnO-Bi_2O_3-xC_3N_4 samples degraded 36.6%, 51.8%, and 30.3% of the Indigo carmine for x = 1, 2 and 3%, respectively. It is evident that the g-C_3N_4 improved significantly the photocatalytic ability of the ZnO-Bi_2O_3. The enhanced photocatalytic activity of heterostructural catalyst ZnO-Bi_2O_3-xC_3N_4 compared to pristine ZnO-Bi_2O_3 might be correlated with the specific Brunauer–Emmett–Teller (BET) surface area. The BET surface areas for ZnO-Bi_2O_3, ZnO-Bi_2O_3-*1*C_3N_4, ZnO-Bi_2O_3-*2*C_3N_4 and ZnO-Bi_2O_3-*3*C_3N_4 were 36.63, 40.20, 44.80 and 49.38 m^2/g, respectively. The measured BET curves BET are shown in Fig. S3. ZnO-Bi_2O_3-*3*C_3N_4 gives higher specific surface area but less photocatalytic activity in comparison with those of ZnO-Bi_2O_3-*1*C_3N_4 and ZnO-Bi_2O_3-*2*C_3N_4. It implies that excessive amount of C_3N_4 presumabley increases the density of C_3N_4 on ZnO-Bi_2O_3 to make the active sites on the ZnO-Bi_2O_3 surface less exposable for photocatalytic reaction.

As expected, the degradation of Indigo carmine was promoted significantly by introducing H_2O_2 to the ZnO-Bi_2O_3-xC_3N_4/Vis system. Fig. 1B shows the photodegradation of Indigo carmine in the presence of ZnO-Bi_2O_3-xC_3N_4 catalysts and H_2O_2. Approximately 8.4% of the Indigo carmine undergoes degradation in the H_2O_2/Vis system within 180 min. In the presence of ZnO-Bi_2O_3-xC_3N_4, the degradation of Indigo carmine was accelerated notably. Under visible light irradiation, approximately 25.2, 38.7, 52.0, 68.8 and 45.3% of Indigo carmine was degraded by pristine ZnO-Bi_2O_3, pristine C_3N_4, ZnO-Bi_2O_3-*1*C_3N_4, ZnO-Bi_2O_3-*2*C_3N_4 and ZnO-Bi_2O_3-*3*C_3N_4, respectively, in the presence of H_2O_2. It reavelaed that H_2O_2 improved significantly Indigo carmine degradation efficiency in the ZnO-Bi_2O_3-xC_3N_4/Vis system. Whereas, the oxidizing abilities of ZnO-Bi_2O_3-xC_3N_4 or H_2O_2 by itself were very weak under visible light irradiation.

As a control experiment, the degradation of Indigo carmine in the ZnO-Bi_2O_3-*2*C_3N_4/H_2O_2/dark system was also tested. Almost no degradation of Indigo carmine was observed when only H_2O_2 was added to the solution without visible light irradiation (~2.7%) (Fig. 1C). Approximately 35.2% of the Indigo carmine was degraded by the ZnO-Bi_2O_3-*2*C_3N_4/H_2O_2/dark system. It is noteworthy that the synergistic effect

between the H_2O_2 and $ZnO\text{-}Bi_2O_3\text{-}2C_3N_4$ under visible light radiation is significant for improving Indigo carmine degradation.

Thus, the hybridization between $g\text{-}C_3N_4$ and $ZnO\text{-}Bi_2O_3$ increased the oxidation rate of Indigo carmine in compared to pristine $ZnO\text{-}Bi_2O_3$. The $g\text{-}C_3N_4$ in $ZnO\text{-}Bi_2O_3\text{-}xC_3N_4$ may improve charge transfer on the heterojunction interfaces. However, an excess amount of $g\text{-}C_3N_4$ affected adversely the photocatalytic activity of $ZnO\text{-}Bi_2O_3\text{-}xC_3N_4$. The reason may be related to the increase of the distribution of $g\text{-}C_3N_4$ in the $ZnO\text{-}Bi_2O_3$, resulting the reduction of the active sites on the $ZnO\text{-}Bi_2O_3$ surface. In addition, excessive $g\text{-}C_3N_4$ may act as mediator for the photoinduced e^- and h^+ recombination, eventually decreasing the photocatalytic activity (Wang et al., 2015). In this study, the activity of the $ZnO\text{-}Bi_2O_3\text{-}2C_3N_4$ photocatalyst was superior to that of the catalysts with other ratios of $g\text{-}C_3N_4$ in terms of the decomposition of Indigo carmine. The photodegradation rate of Indigo carmine over the $ZnO\text{-}Bi_2O_3\text{-}2C_3N_4/H_2O_2$/Vis system was significantly higher than that of the $ZnO\text{-}Bi_2O_3/H_2O_2$/Vis system by about 5.6 times.

To obtain quantitative point of view into the reaction kinetics of Indigo carmine degradation, a typical first-order model was applied to fit the experimental data. The first-order kinetics can be expressed as $\ln(C_0/C_t) = kt$, where t is the reaction time (min), k is the rate constant (min^{-1}), and C_0 and C_t are the Indigo carmine concentrations (mg/L) at the time of $t = 0$ and $t = t$, respectively. The fitted plots and rate constant k values of all the tested samples are shown in Fig. 2.

Accordingly, the reaction rate constant k values help to evaluate the degradation rates. It can be found that the $ZnO\text{-}Bi_2O_3\text{-}2C_3N_4$ exhibited the highest performance during the degradation of Indigo carmine with and without adding H_2O_2 over 180 min visible light irradiation. As seen in Fig. 2A, the k value of $ZnO\text{-}Bi_2O_3\text{-}2C_3N_4$ was found to be 0.0037 min^{-1}, which was almost 9.3-fold, 1.6-fold and 1.9-fold higher than that of $ZnO\text{-}Bi_2O_3$ (0.0004 min^{-1}), $ZnO\text{-}Bi_2O_3\text{-}1C_3N_4$ (0.0022 min^{-1}) and $ZnO\text{-}Bi_2O_3\text{-}3C_3N_4$ (0.0019 min^{-1}), respectively. In the presence of H_2O_2, the rate constant k values of Indigo carmine degradation over 180 min under visible light irradiation were found to be 0.001 min^{-1} for $ZnO\text{-}Bi_2O_3$, 0.0036 min^{-1} for $ZnO\text{-}Bi_2O_3\text{-}1C_3N_4$, 0.0056 min^{-1} for $ZnO\text{-}Bi_2O_3\text{-}2C_3N_4$ and 0.0032 min^{-1} for $ZnO\text{-}Bi_2O_3\text{-}3C_3N_4$ (Fig. 2B). In contract, the $ZnO\text{-}Bi_2O_3\text{-}2C_3N_4/H_2O_2$/dark system, the k values of Indigo carmine degradation without visible light irradiation was found to be 0.0021 min^{-1} (Fig. 2C). The results in Fig. 2 revealed that Indigo carmine degradation in the $ZnO\text{-}Bi_2O_3\text{-}2C_3N_4/H_2O_2$/-dark system is 2.7 times and 1.8 times lower than those in the $ZnO\text{-}Bi_2O_3\text{-}2C_3N_4/H_2O_2$/Vis and $ZnO\text{-}Bi_2O_3\text{-}2C_3N_4$/Vis

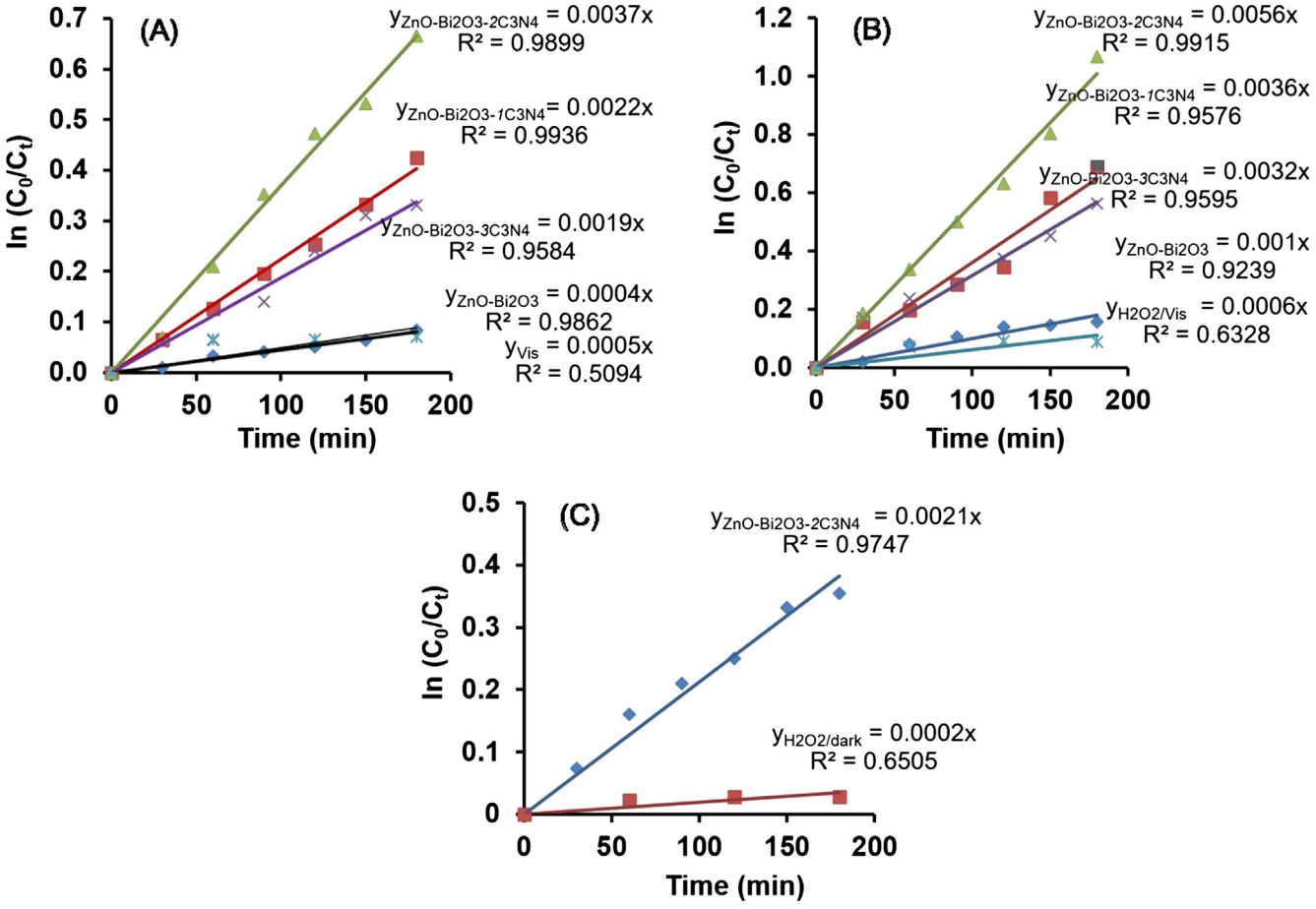

Fig. 2 The first-order plots for Indigo carmine degradation in the (A) $ZnO\text{-}Bi_2O_3\text{-}xC_3N_4$/Vis system; (B) $ZnO\text{-}Bi_2O_3\text{-}xC_3N_4/H_2O_2$/Vis system and (C) $ZnO\text{-}Bi_2O_3\text{-}xC_3N_4/H_2O_2$/dark system.

system, respectively. The order of Indigo carmine degradation is ZnO-Bi_2O_3-xC_3N_4/H_2O_2/Vis system > ZnO-Bi_2O_3-xC_3N_4/Vis system > ZnO-Bi_2O_3-xC_3N_4 /H_2O_2/dark system.

3.2. Catalytic activity of ZnO-Bi_2O_3-$2C_3N_4$/H_2O_2/Vis system

3.2.1. Effect of the loading of ZnO-Bi_2O_3-$2C_3N_4$ and pH value

Fig. 3A illustrates the degradation of Indigo carmine (50 mg/L) in the ZnO-Bi_2O_3-$2C_3N_4$/H_2O_2/Vis system with various loads of ZnO-Bi_2O_3-$2C_3N_4$, keeping the concentration of H_2O_2 constant (2.14 mmol/L) at pH 7.0. Compared with the H_2O_2/Vis system (i.e., a zero load of ZnO-Bi_2O_3-$2C_3N_4$), the degradation of Indigo carmine enhanced significantly by the addition of ZnO-Bi_2O_3-$2C_3N_4$, because ZnO-Bi_2O_3-$2C_3N_4$ can act as a peroxidase-like catalyst to accelerate the decomposition of H_2O_2, thus enabling the creation of strongly oxidizing radical species. When the amount of ZnO-Bi_2O_3-$2C_3N_4$ was increased from 0.5 to 2.0 g/L, the rate constant k of Indigo carmine degradation greatly increased from 0.0056 to 0.0101 min^{-1} (Fig. 3B). Beyond the ZnO-Bi_2O_3-$2C_3N_4$ loading of 2.0 g/L, k is decreased; this may be due to excessive amount of catalyst, which caused the solution to become opaque. This would allow less light to pass through the solution, which hinders the Indigo carmine degradation reaction.

Fig. 3C shows the degradation of Indigo carmine in the ZnO-Bi_2O_3-$2C_3N_4$/H_2O_2/Vis system with different initial pH values in the solution (pH 2, 3, 5, 7, and 8), while the concentration of ZnO-Bi_2O_3-$2C_3N_4$ and H_2O_2 were fixed at 2.0 g/L and 2.14 mmol/L, respectively. As seen in Fig. 3C, the catalytic system of ZnO-Bi_2O_3-$2C_3N_4$/H_2O_2/Vis can degrade Indigo carmine across a wide range of pH values. The degradation of Indigo carmine was enhanced gradually at pH values ranging from pH 2 to pH 7, but reduced at pH 8. The order of the degradation rate of Indigo carmine by ZnO-Bi_2O_3-$2C_3N_4$/H_2O_2/Vis at different pH values is as follows: pH 7 (k = 0.0101 min^{-1}) > pH 5 (k = 0.0073 min^{-1}) > pH 3 (k = 0.0065 min^{-1}) ~ pH 2 (k = 0.0064 min^{-1}) > pH 8 (k = 0.0042 min^{-1}) (Fig. 3D). This can be understood by considering that, the larger concentration of OH^- groups in solution hinders the movement of the Indigo carmine anion and its ability to make contact with the catalyst surface at pH greater than 7, leading to a decrease in the degradation rate.

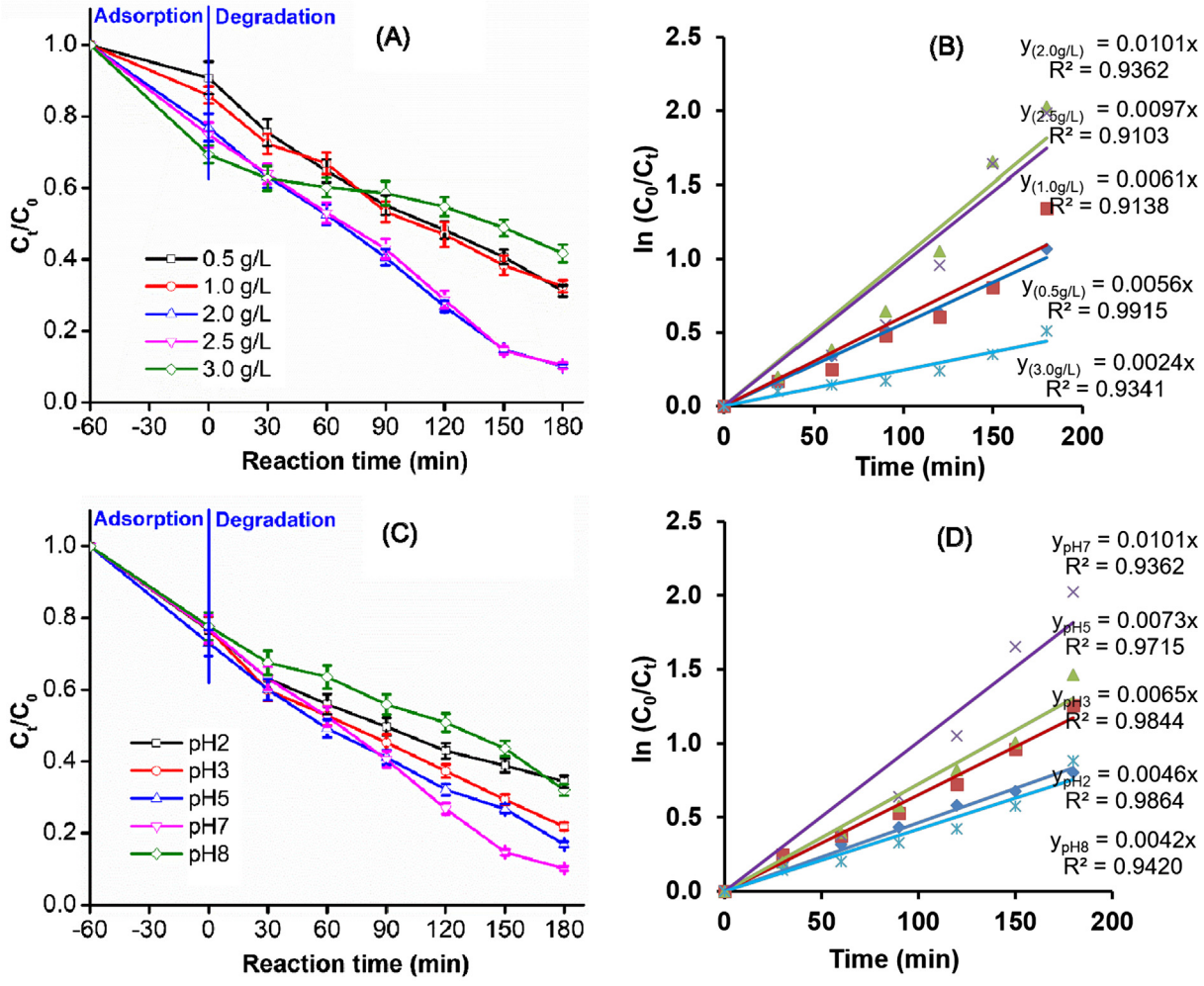

Fig. 3 Photodegradation of Indigo carmine over ZnO-Bi_2O_3-$2C_3N_4$/H_2O_2/Vis system: (A) effect of the loading of ZnO-Bi_2O_3-$2C_3N_4$, (B) the first-order plots for Indigo carmine degradation using different amount of ZnO-Bi_2O_3-$2C_3N_4$, (C) effect of pH of the solution, and (D) The first-order plots for Indigo carmine degradation at different pH values.

3.2.2. Effect of H_2O_2 concentration and photocatalytic stability of ZnO-Bi_2O_3-2C_3N_4

The main problem in most of the photocatalytic processes is the unwanted recombination of electrons/holes. This represents a major energy waste and feasible quantum yield limitation. The H_2O_2 is an electron donor that not only facilitates photocatalytic processes but also inhibits electron-hole pair recombination (Tseng et al., 2012). The effect of H_2O_2 concentration on the photocatalytic degradation of Indigo carmine was thus examined in this sense, while the quantity of ZnO-Bi_2O_3-2C_3N_4 and pH solution were maintained at 2.0 g/L and 7.0, respectively. Fig. 4A displays the degradation of Indigo carmine in the ZnO-Bi_2O_3-2C_3N_4/H_2O_2/Vis system with different initial concentrations of H_2O_2. Without H_2O_2, Indigo carmine was hardly degraded. This indicates that the presence of ZnO-Bi_2O_3-2C_3N_4 alone cannot produce sufficient amounts of reactive radical species under visible light irradiation. The addition of H_2O_2 is necessary to enhance the Indigo carmine degradation. As the H_2O_2 concentration was increased from 1.07 to 4.28 mmol/L, the rate constant k of Indigo carmine degradation was greatly increased up to 0.0028 and 0.0119 min^{-1} in ZnO-Bi_2O_3-2C_3N_4/H_2O_2/Vis (Fig. 3B). It is noted that the k values tend to decrease in the ZnO-Bi_2O_3-2C_3N_4/H_2O_2/Vis system when the H_2O_2 concentration exceeded 4.28 mmol/L, revealing that an excessive amount of H_2O_2 on the surface of ZnO-Bi_2O_3-2C_3N_4 was not favorable for Indigo carmine degradation. This is ascribed to the fact that H_2O_2 mainly acts as a source of hydroxyl radicals (OH·) and as an electron scavenger to inhibit electron-hole recombination at low concentration (Dostanic et al. 2011):

$$H_2O_2 + e^- \rightarrow OH\cdot + OH^- \quad (1)$$

However, at high concentration, excess H_2O_2 may act as a radical scavenger. The generated reactive radicals (OH·) may react with excess H_2O_2 to form hydroperoxyl radicals (OOH·) of which the oxidation potential is much lower compared to that of OH·. Then it reduces the reactive radicals available for the Indigo carmine oxidation, leading to a decrease in the photocatalytic efficiency (Wang et al., 2010, Pang and Abdullah, 2013):

$$H_2O_2 + OH\cdot \rightarrow H_2O + OOH\cdot \quad (2)$$

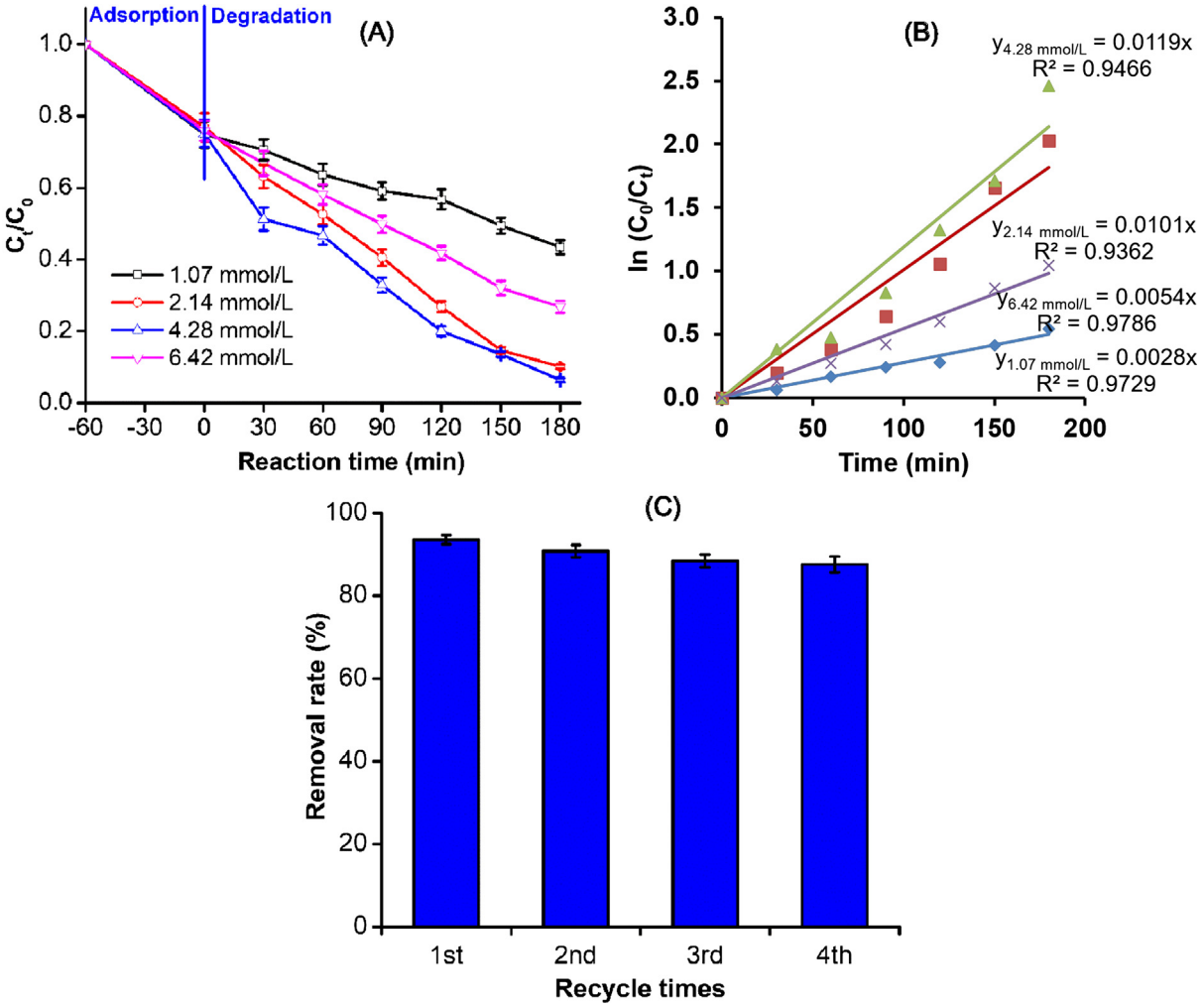

Fig. 4 Degradation of Indigo carmine over ZnO-Bi_2O_3-2C_3N_4/H_2O_2/Vis system (A) effect of the initial H_2O_2 concentration and (B) the first-order plots for Indigo carmine degradation using different H_2O_2 concentration; (C) reusability of ZnO-Bi_2O_3-2C_3N_4 over ZnO-Bi_2O_3-2C_3N_4/H_2O_2/Vis system (180 min of visible light irradiation; pH 7; solid/liquid ratio of 2.0 g/L; initial Indigo carmine and H_2O_2 concentration of 50 mg/L and 4.28 mM, respectively).

Thus, more than 93.6% of the Indigo carmine solution (50 mg/L) was degraded by ZnO-Bi_2O_3-2C_3N_4 (2.0 g/L) with the assistance of H_2O_2 (4.28 mmol/L) over 180 min under visible light irradiation at pH 7.0. Similar results were reported by others, namely that a high H_2O_2 dosage had an undesired impact on the reaction kinetics, which decreased to almost zero on kinetic heterogeneous photocatalysis (Gemeay et al., 2003). The photodegradation capability of the ZnO-Bi_2O_3-2C_3N_4/H_2O_2/Vis system was significantly improved in comparison with previous reports (Palma-Goyes et al., 2014, Liu et al., 2015).

The mineralization of Indigo carmine with the ZnO-Bi_2O_3-2C_3N_4/H_2O_2/Vis system was clarified by the total organic carbon (TOC) in the solution using a Shimadzu TOC-VCPH analyzer (Japan). In addition, the TOC in the ZnO-Bi_2O_3-2C_3N_4 before and after light irradiation were also measured. The calculation of TOC mass balance is presented in Table 1.

The TOC removal (%) was calculated with the following equation:

$$TOC_{removal}(\%) = \frac{TOC_{in} - TOC_{re}}{TOC_{in}} \times 100 \quad (3)$$

where TOC_{in} (mg) refer to the initial TOC values; TOC_{re} (mg) refer to the remaining TOC in solution and on ZnO-Bi_2O_3-2C_3N_4 after visible light irradiation.

From the Eq. (3), the amount of TOC removal reached 84.76% for the ZnO-Bi_2O_3-2C_3N_4/H_2O_2/Vis system after 180 min under visible light irradiation, confirming that the outstanding mineralization ability of the ZnO-Bi_2O_3-2C_3N_4/H_2O_2/Vis system. Before visible light irradiation, there was about 0.51 mg (~24.29%) TOC absorbed on ZnO-Bi_2O_3-2C_3N_4, however, only 0.10 mg (~4.76%) of TOC remained on ZnO-Bi_2O_3-2C_3N_4 after the irradiation of visible light for 180 min. The different amount of TOC on ZnO-Bi_2O_3-2C_3N_4 before and after the irradiation indicates that the desorption occurred during photodegradation. ZnO-Bi_2O_3-2C_3N_4 was almost free from Indigo carmine after the irradiation for 180 min. The mineralization performance of the Fe^{2+}/UV/H_2O_2 system was approximately 42% of Indigo carmine (20 mg/L solution at pH 5.6 in the presence of 2.03 mmol/L of H_2O_2 after 60 min irradiation) (Palma-Goyes et al., 2014).

The study on photochemical stability of ZnO-Bi_2O_3-2C_3N_4/H_2O_2/Vis system was performed. The results shown in Fig. 4C confirm that the high stability of ZnO-Bi_2O_3-2C_3N_4 although the catalyst were recycled four times in succession and decreasing after the fourth consecutive cycles was very small. Approximately 87.6% of Indigo carmine was successfully photodegraded after fourth run to indicate that the loss in photocatalytic performance of ZnO-Bi_2O_3-2C_3N_4 was negligible after four recycling runs.

3.3. Photodegradation mechanism

The hybridization between ZnO-Bi_2O_3 with C_3N_4 formed a heterostructural semiconductor system to result in an effective photogenerated e^-- h^+ pair separation and the generation of the photodegradation sites. Degradation of Indigo carmine by the ZnO-Bi_2O_3-2C_3N_4/H_2O_2/Vis system is mainly due to $OH^{\cdot}$ and $O_2^{\cdot-}$ radicals. Thus, the reaction mechanisms were further examined by using two scavengers for determining the active species in the photocatalytic process. The photodegradation of Indigo carmine is limited clearly after the ethanol injection as a $OH^{\cdot}$ radicals scavenger, as shown in Fig. 5A. The rate constant (k) in the ZnO-Bi_2O_3-2C_3N_4/H_2O_2/Vis system is reduced from 0.0119 min^{-1} to 0.0004 min^{-1} with the addition of $OH^{\cdot}$ radical scavengers (Fig. 5B). The more the k value is reduced, the more important role of the corresponding oxidative species in the reaction. Indeed, only 28.2% of Indigo carmine was degraded in the ZnO-Bi_2O_3-2C_3N_4/H_2O_2/Vis system after 180 min without $OH^{\cdot}$ radicals. The influence of ascorbic acid as a scavenger of $O_2^{\cdot-}$ radicals is not worthy of attention on the degradation rate of Indigo carmine. The rate constant (k) is 0.0095 min^{-1} and 88.5% of Indigo carmine photodegradation was attained after 180 min.

It is well known that the hybridization of semiconductors with different redox energy levels of conduction band (CB) and valence band (VB) may improve the efficiency of photogenerated e^- - h^+ pair separation and charge transfer at the interface (Yan et al., 2016). To assess the mechanism for the enhancement of photocatalytic activity in ZnO-Bi_2O_3-2C_3N_4 sample, the conduction band (CB) and valence band (VB) of the semiconductors were calculated using the following formulas (Cui et al., 2014, Xu et al., 2015):

$$E_{VB} = X - E^e + 0.5E_g \quad (4)$$

$$E_{CB} = E_{VB} - E_g \quad (5)$$

where E_{CB} and E_{VB} are the conduction band and valence band potential, respectively. x is the electronegativity of ZnO and ZnO-Bi_2O_3 (ca. 5.79 eV for ZnO and 6.11 eV for ZnO-Bi_2O_3) and E^e is the energy of free electrons on the hydrogen scale (ca. 4.5 eV). The band gap energies of the impurity of ZnO, ZnO-Bi_2O_3 and C_3N_4 were calculated and reported in our previous paper (Bui et al., 2017). It was found that the band gap energies of the impurity of ZnO, ZnO-Bi_2O_3 and C_3N_4 are 2.95, 2.20 and 2.67 eV, respectively. The E_{VB} and E_{CB} values were approximately 2.77 and −0.18 eV with the ZnO impurity, 2.71 and 0.51 eV for ZnO-Bi_2O_3, and 1.57 and −1.10 eV for C_3N_4, respectively. However, the E_{VB} and E_{CB} was normally able to change with pH. The new E_{VB} and E_{CB} for ZnO,

Table 1 Mass balance of TOC in the reactor over ZnO-Bi_2O_3-2C_3N_4/H_2O_2/Vis system (reaction condition: 100 mL Indigo carmine 50 mg/L, ZnO-Bi_2O_3-2C_3N_4 2.0 g/L, H_2O_2 4.28 mmol/L, pH 7.0).

TOC in solution (mg)			TOC in ZnO-Bi_2O_3-2C_2N_3 (mg)		Total TOC remaining in reactor (mg)
Initial	Before irradiation	After irradiation	Before irradiation	After irradiation	
2.10 ± 0.06	1.58 ± 0.10	0.22 ± 0.03	0.51 ± 0.04	0.10 ± 0.01	0.32

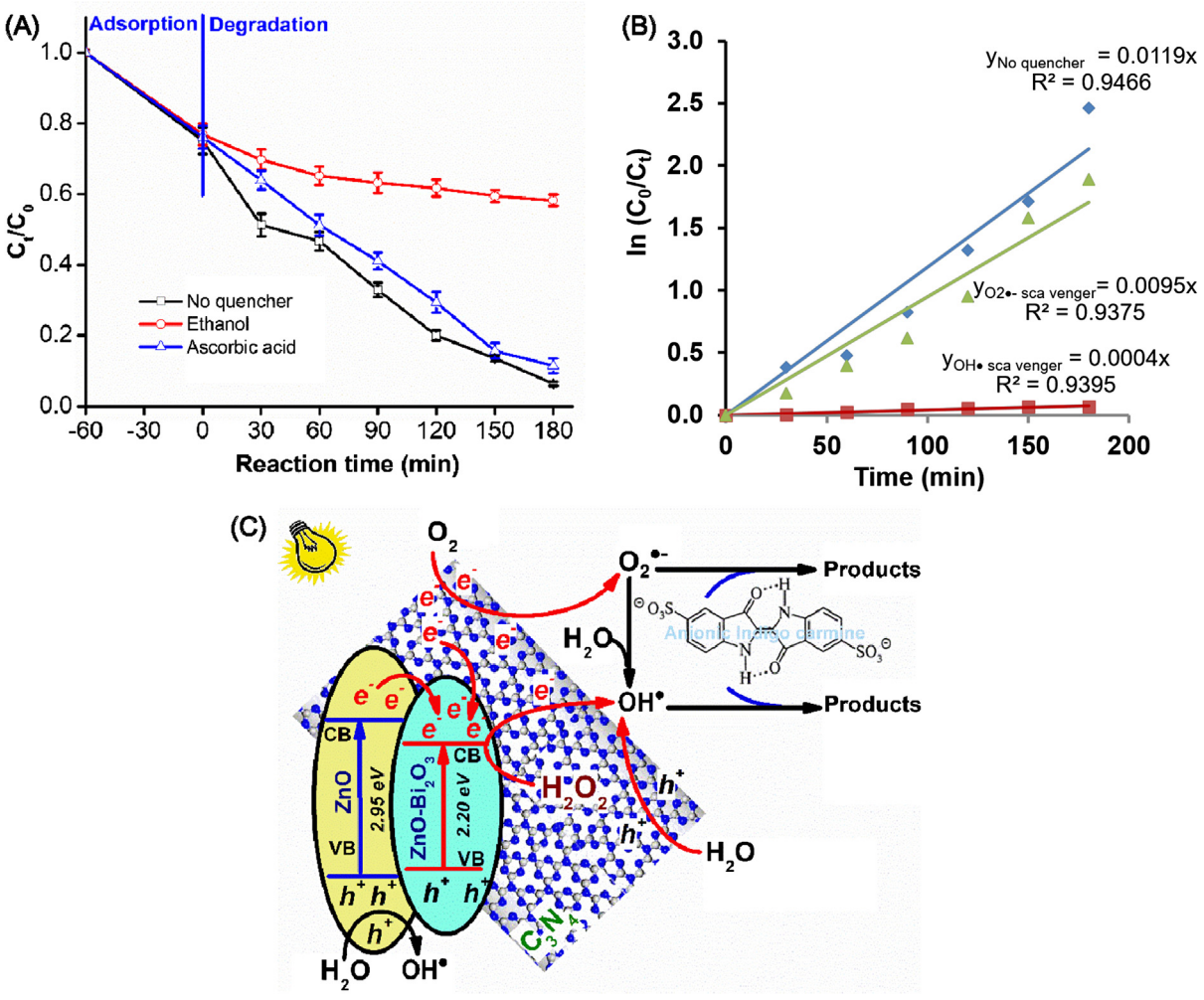

Fig. 5 (A) Degradation of Indigo carmine over the ZnO-Bi_2O_3-2C_3N_4/H_2O_2/Vis system with the addition of OH· and $O_2^{\cdot-}$ radical scavengers and (B) The first-order plots for Indigo carmine degradation with the addition of OH· and $O_2^{\cdot-}$ radical scavengers; (C) Degradation mechanisms of Indigo carmine by the ZnO-Bi_2O_3-2C_3N_4/H_2O_2/Vis system.

ZnO-Bi_2O_3 and C_3N_4 at pH 7.0 were calculated using the following formula (Zhu et al., 2017):

$$E = E^{\circ} + 0.05915log[H^+] = E^{\circ} - 0.05915pH \quad (6)$$

where E° is the band potential of the photocatalyst at pH 0. The E_{VB} and E_{CB} were found to be 2.36 and −0.59 eV for ZnO, 2.30 and 0.10 eV for ZnO-Bi_2O_3, and 1.16 and −1.51 eV for C_3N_4, respectively. The E_{CB} and E_{VB} of C_3N_4 and ZnO were higher than those of ZnO-Bi_2O_3 to result the advantageous for the separation and transportation of charge carriers.

The mechanism of the charge-carriers separation is presented in Fig. 5C to describe the enriched activity of ZnO-Bi_2O_3-2C_3N_4 as well as the degradation of Indigo carmine on the ZnO-Bi_2O_3-2C_3N_4/H_2O_2/Vis systems. The strong electronic coupling between ZnO-Bi_2O_3 and C_3N_4, and the heterojunction structure can effectively produce the photogenerated e^- - h^+ pairs under visible light irradiation. Due to the CB edge potential of C_3N_4 (−1.45 eV) and impurity ZnO (−0.46 eV) are more negative than those of ZnO-Bi_2O_3, they can directly transfer into the CB of ZnO-Bi_2O_3 through its alternate conjugation as soon as the excited state e^- of C_3N_4 and impurity ZnO generated, whereas h^+ accumulated on the VB. Because H_2O_2 scavenges photogenerated e^- rapidly to generate OH· radicals, direct e^- - h^+ recombination is likely prevented, which enhances the photocatalytic activity. In addition, the photogenerated e^- can react with O_2 adsorbed onto ZnO-Bi_2O_3 to form $O_2^{\cdot-}$ radicals. Similarly, the photogenerated h^+ on the VB of impurity ZnO, ZnO-Bi_2O_3 and C_3N_4 can directly react with H_2O to generate OH· radicals. The formed OH· and $O_2^{\cdot-}$ radicals could efficiently mineralize Indigo carmine into CO_2 and water. Thus, the ZnO-Bi_2O_3 in ZnO-Bi_2O_3-C_3N_4 can act as photogenerated e^- acceptors because of charge transportation. A similar effect was reported by Benalioua's group, who studied the strong synergistic combination of TiO_2 and BiZn-LDH under visible irradiation (Benalioua et al., 2015). The hybridization of ZnO-Bi_2O_3 with C_3N_4 plays an important role in photocatalytic efficiency, which is attributed to the synergistic effect of chemical contact as well as electron and hole transport from C_3N_4 to ZnO-Bi_2O_3.

The mechanism for the degradation of Indigo carmine by the ZnO-Bi_2O_3-2C_3N_4/H_2O_2/Vis system can be described by the following reactions:

$$ZnO\text{-}Bi_2O_3\text{-}2C_3N_4 + hv \rightarrow ZnO\text{-}Bi_2O_3\text{-}2C_3N_4\ (e^- + h^+) \quad (7)$$

$$ZnO\text{-}Bi_2O_3\text{-}2C_3N_4\ (e^-) + H_2O_2 \rightarrow OH^{\cdot} + OH^- \quad (8)$$

$$ZnO\text{-}Bi_2O_3\text{-}2C_3N_4\ (e^-) + O_2 \rightarrow O_2^{\cdot -} \quad (9)$$

$$O_2^{\cdot -} + 2H_2O \rightarrow 2OH^{\cdot} + 2OH^- \quad (10)$$

$$ZnO\text{-}Bi_2O_3\text{-}2C_3N_4\ (h^+) + 2H_2O \rightarrow OH^{\cdot} + H^+ \quad (11)$$

$$OH^{\cdot} + \text{Indigo carmine} \rightarrow \text{degradation products} \rightarrow CO_2 + H_2O(\text{Majorreaction}) \quad (12)$$

$$O_2^{\cdot -} + \text{Indigo carmine} \rightarrow \text{degradation products} \rightarrow CO_2 + H_2O(\text{Minorreaction}) \quad (13)$$

$$h^+ + e^- \rightarrow (e^-, h^+)\ (\text{negligible recombination reaction}) \quad (14)$$

4. Conclusions

We developed an enhanced photocatalytic system of ZnO-Bi_2O_3-$2C_3N_4$ and applied for degrading Indigo carmine in aqueous solution by the aid of H_2O_2 under visible light irradiation. The ZnO-Bi_2O_3-$2C_3N_4$/H_2O_2/Vis system degraded Indigo carmine with high efficiency (93% of Indigo carmine in 180 min). This strong synergistic effect is ascribed to the promotion of heterogeneous catalysis in ZnO-Bi_2O_3-$2C_3N_4$ by the irradiation of visible light as a result of improved transfer of the photogenerated e^- and h^+ at the heterojunction interface between ZnO-Bi_2O_3 and g-C_3N_4, which reduces the recombination of e^- - h^+ pairs. The photogenerated e^- and h^+ react rapidly with H_2O_2, H_2O, and adsorbed O_2 to generate $OH^{\cdot}$ and $O_2^{\cdot -}$ radicals. Efforts to identify the active species indicated that $OH^{\cdot}$ radicals are the major species responsible for complete mineralization with the minor contributions by $O_2^{\cdot -}$ radicals. In addition, ZnO-Bi_2O_3-$2C_3N_4$ displayed excellent stability during four successive experimental cycles.

Acknowledgements

This research was supported by the Basic Science Research Program through the National Research Foundation of Korea (NRF) funded by the Ministry of Education (NRF-2017R1A2B4006388) and (NRF-2017R1D1A3B03035530).

Conflict of interest

The authors declare no competing financial interest.

Appendix A. Supplementary materail

Supporting information consists of the synthetic procedure, characterization of the samples. Supplementary data to this article can be found online at https://doi.org/10.1016/j.arabjc.2019.01.003.

References

Barka, N., Assabbane, A., Nounah, A., Ichou, Y.A., 2008. Photocatalytic degradation of indigo carmine in aqueous solution by TiO_2-coated non-woven fibres. J. Hazard. Mater. 152 (3), 1054–1059. https://doi.org/10.1016/j.jhazmat.2007.07.080.

Benalioua, B., Mansour, M., Bentouami, A., Boury, B., Elandaloussi, E.H., 2015. The layered double hydroxide route to Bi–Zn co-doped TiO_2 with high photocatalytic activity under visible light. J. Hazard. Mater. 288, 158–167. https://doi.org/10.1016/j.jhazmat.2015.02.013.

Bui, T.H., Thi Bich Thao, C., Dao, V.-D., Phuong, N., Lee, Y.-I., 2017. A mixed-metal oxides/graphitic carbon nitride: high visible light photocatalytic activity for efficient mineralization of rhodamine B. Adv. Mater. Interfaces 4, 1700128. https://doi.org/10.1002/admi.201770057.

Cao, J., Xu, B., Lin, H., Luo, B., Chen, S., 2012. Novel Bi_2S_3-sensitized BiOCl with highly visible light photocatalytic activity for the removal of rhodamine B. Catal. Commun. 26, 204–208. https://doi.org/10.1016/j.catcom.2012.05.025.

Centi, G., Perathoner, S., Torre, T., Verduna, M.G., 2000. Catalytic wet oxidation with H_2O_2 of carboxylic acids on homogeneous and heterogeneous Fenton-type catalysts. Catal. Today 55 (1), 61–69. https://doi.org/10.1016/S0920-5861(99)00226-6.

Chai, B., Peng, T., Mao, J., Li, K., Zan, L., 2012. Graphitic carbon nitride (g-C_3N_4)-Pt-TiO_2 nanocomposite as an efficient photocatalyst for hydrogen production under visible light irradiation. Phys. Chem. Chem. Phys. 14 (48), 16745–16752. https://doi.org/10.1039/c2cp42484c.

Chen, P., Wang, H., Liu, H., Ni, Z., Li, J., Zhou, Y., Dong, F., 2019. Directional electron delivery and enhanced reactants activation enable efficient photocatalytic air purification on amorphous carbon nitride co-functionalized with O/La. Appl. Catal.B 242, 19–30. https://doi.org/10.1016/j.apcatb.2018.09.078.

Chunyan, Z., Yongfeng, L., Qingqing, J., Juncheng, H., 2016. Synthesis of CdS hollow spheres coupled with g-C 3 N 4 as efficient visible-light-driven photocatalysts. Nanotechnology 27 (35), 355402. https://doi.org/10.1088/0957-4484/27/35/355402.

Cui, W., Li, J., Sun, Y., Wang, H., Jiang, G., Lee, S.C., Dong, F., 2018. Enhancing ROS generation and suppressing toxic intermediate production in photocatalytic NO oxidation on O/Ba co-functionalized amorphous carbon nitride. Appl. Catal. B 237, 938–946. https://doi.org/10.1016/j.apcatb.2018.06.071.

Cui, Y., Jia, Q., Li, H., Han, J., Zhu, L., Li, S., Zou, Y., Yang, J., 2014. Photocatalytic activities of Bi_2S_3/BiOBr nanocomposites synthesized by a facile hydrothermal process. Appl. Surf. Sci. 290, 233–239. https://doi.org/10.1016/j.apsusc.2013.11.055.

Ding, G., Wang, W., Jiang, T., Han, B., Fan, H., Yang, G., 2013. Highly selective synthesis of phenol from benzene over a vanadium-doped graphitic carbon nitride catalyst. ChemCatChem 5 (1), 192–200. https://doi.org/10.1002/cctc.201200502.

Dong, X.a., Li, J., Xing, Q., Zhou, Y., Huang, H., Dong, F., 2018. The activation of reactants and intermediates promotes the selective photocatalytic NO conversion on electron-localized Sr-intercalated g-C_3N_4. Appl. Catal. B 232, 69–76. https://doi.org/10.1016/j.apcatb.2018.03.054.

Dostanic, J., Loncarevic, D., Banković, P., Cvetkovic, O., Jovanović, D., Mijin, D., 2011. Influence of process parameters on the photodegradation of synthesized azo pyridone dye in TiO_2 water suspension under simulated sunlight. J. Environ. Sci. Health Part A: Toxic/Hazard. Subst. Environ. Eng. 46 (1), 70–79. https://doi.org/10.1080/10934529.2011.526905.

Fu, J., Chang, B., Tian, Y., Xi, F., Dong, X., 2013. Novel C_3N_4-CdS composite photocatalysts with organic-inorganic heterojunctions: in situ synthesis, exceptional activity, high stability and photocatalytic mechanism. J. Mater. Chem. A 1 (9), 3083–3090. https://doi.org/10.1039/c2ta00672c.

Gemeay, A.H., Mansour, I.A., El-Sharkawy, R.G., Zaki, A.B., 2003. Kinetics and mechanism of the heterogeneous catalyzed oxidative degradation of indigo carmine. J. Mol. Catal. A: Chem. 193 (1), 109–120. https://doi.org/10.1016/S1381-1169(02)00477-6.

Hu, S.W., Yang, L.W., Tian, Y., Wei, X.L., Ding, J.W., Zhong, J.X., Chu, P.K., 2014. Non-covalent doping of graphitic carbon nitride with ultrathin graphene oxide and molybdenum disulfide nanosheets: An effective binary heterojunction photocatalyst under visible light irradiation. J. Colloid Interface Sci. 431, 42–49. https://doi.org/10.1016/j.jcis.2014.05.023.

Irmak, S., Yavuz, H.I., Erbatur, O., 2006. Degradation of 4-chloro-2-methylphenol in aqueous solution by electro-Fenton and photo-electro-Fenton processes. Appl. Catal., B 63 3–4, 243–248. https://doi.org/10.1016/j.apcatb.2005.10.008.

Jiang, S., Zhou, K., Shi, Y., Lo, S., Xu, H., Hu, Y., Gui, Z., 2014. In situ synthesis of hierarchical flower-like Bi_2S_3/BiOCl composite with enhanced visible light photocatalytic activity. Appl. Surf. Sci. 290, 313–319. https://doi.org/10.1016/j.apsusc.2013.11.074.

Kim Phuong, N.T., Beak, M.-W., Huy, B.T., Lee, Y.-I., 2016. Adsorption and photodegradation kinetics of herbicide 2,4,5-trichlorophenoxyacetic acid with MgFeTi layered double hydroxides. Chemosphere 146, 51–59. https://doi.org/10.1016/j.chemosphere.2015.12.008.

Li, J., Zhang, Z., Cui, W., Wang, H., Cen, W., Johnson, G., Jiang, G., Zhang, S., Dong, F., 2018a. The spatially oriented charge flow and photocatalysis mechanism on internal van der Waals heterostructures enhanced g-C_3N_4. ACS Catal. 8 (9), 8376–8385. https://doi.org/10.1021/acscatal.8b02459.

Li, Y., Sun, Y., Ho, W., Zhang, Y., Huang, H., Cai, Q., Dong, F., 2018b. Highly enhanced visible-light photocatalytic NOx purification and conversion pathway on self-structurally modified g-C_3N_4 nanosheets. Sci. Bull. 63 (10), 609–620. https://doi.org/10.1016/j.scib.2018.04.009.

Liu, H., Jin, Z., Su, Y., Wang, Y., 2015. Visible light-driven $Bi_2Sn_2O_7$/reduced graphene oxide nanocomposite for efficient photocatalytic degradation of organic contaminants. Sep. Purif. Technol. 142, 25–32. https://doi.org/10.1016/j.seppur.2014.12.027.

Mendoza-Damián, G., Tzompantzi, F., Mantilla, A., Barrera, A., Lartundo-Rojas, L., 2013. Photocatalytic degradation of 2,4-dichlorophenol with MgAlTi mixed oxides catalysts obtained from layered double hydroxides. J. Hazard. Mater. 263 (Part 1), 67–72. https://doi.org/10.1016/j.jhazmat.2013.09.047.

Mohapatra, L., Parida, K.M., 2014. Dramatic activities of vanadate intercalated bismuth doped LDH for solar light photocatalysis. Phys. Chem. Chem. Phys. 16 (32), 16985–16996. https://doi.org/10.1039/C4CP01665C.

Nayak, S., Parida, K.M., 2018. Dynamics of charge-transfer behavior in a plasmon-induced quasi-type-II p–n/n–n dual heterojunction in Ag@Ag_3PO_4/g-C_3N_4/NiFe LDH nanocomposites for photocatalytic Cr(VI) reduction and phenol oxidation. ACS Omega 3 (7), 7324–7343. https://doi.org/10.1021/acsomega.8b00847.

Oturan, M.A., Peiroten, J., Chartrin, P., Acher, A.J., 2000. Complete destruction of p-nitrophenol in aqueous medium by electro-fenton method. Environ. Sci. Technol. 34 (16), 3474–3479. https://doi.org/10.1021/es990901b.

Palma-Goyes, R.E., Silva-Agredo, J., González, I., Torres-Palma, R. A., 2014. Comparative degradation of indigo carmine by electrochemical oxidation and advanced oxidation processes. Electrochim. Acta 140, 427–433. https://doi.org/10.1016/j.electacta.2014.06.096.

Pang, Y.L., Abdullah, A.Z., 2013. Fe^{3+} doped TiO_2 nanotubes for combined adsorption–sonocatalytic degradation of real textile wastewater. Appl. Catal. B 129, 473–481. https://doi.org/10.1016/j.apcatb.2012.09.051.

Patnaik, S., Das, K.K., Mohanty, A., Parida, K., 2018a. Enhanced photo catalytic reduction of Cr (VI) over polymer-sensitized g-C_3N_4/$ZnFe_2O_4$ and its synergism with phenol oxidation under visible light irradiation. Catal. Today 315, 52–66. https://doi.org/10.1016/j.cattod.2018.04.008.

Patnaik, S., Sahoo, D.P., Mohapatra, L., Martha, S., Parida, K., 2017. $ZnCr_2O_4$@ZnO/g-C_3N_4: a triple-junction nanostructured material for effective hydrogen and oxygen evolution under visible light. Energy Technol. 5 (9), 1687–1701. https://doi.org/10.1002/ente.201700071.

Patnaik, S., Sahoo, D.P., Parida, K., 2018b. An overview on Ag modified g-C_3N_4 based nanostructured materials for energy and environmental applications. Renew. Sustain. Energy Rev. 82, 1297–1312. https://doi.org/10.1016/j.rser.2017.09.026.

Patnaik, S., Swain, G., Parida, K.M., 2018c. Highly efficient charge transfer through a double Z-scheme mechanism by a Cu-promoted MoO_3/g-C_3N_4 hybrid nanocomposite with superior electrochemical and photocatalytic performance. Nanoscale 10 (13), 5950–5964. https://doi.org/10.1039/C7NR09049H.

Ruiru, Z., Jianping, G., Shunkang, M., Yongli, W., Xiaoxue, W., Xiangang, Z., Jiangbing, Y., Chaoyue, H., Jing, Y., 2017. Facile synthesis of graphitic C 3 N 4 nanoporous-tube with high enhancement of visible-light photocatalytic activity. Nanotechnology 28, (49) <https://doi.org.org/10.1088/1361-6528/aa929a> 495710.

Shi, Y., Wang, B., Duan, L., Zhu, Y., Gui, Z., Yuen, R.K.K., Hu, Y., 2016. Processable dispersions of graphitic carbon nitride based nanohybrids and application in polymer nanocomposites. Ind. Eng. Chem. Res. 55 (28), 7646–7654. https://doi.org/10.1021/acs.iecr.6b01237.

Tseng, D.-H., Juang, L.-C., Huang, H.-H., 2012. Effect of oxygen and hydrogen peroxide on the photocatalytic degradation of monochlorobenzene in aqueous suspension. Int. J. Photoenergy 2012, 9. https://doi.org/10.1155/2012/328526.

Virkutyte, J., Varma, R.S., 2014. Eco-friendly magnetic iron oxide-pillared montmorillonite for advanced catalytic degradation of dichlorophenol. ACS Sustain. Chem. Eng. 2 (7), 1545–1550. https://doi.org/10.1021/sc5002512.

Wang, H., Yuan, X., Wu, Y., Zeng, G., Chen, X., Leng, L., Li, H., 2015. Synthesis and applications of novel graphitic carbon nitride/metal-organic frameworks mesoporous photocatalyst for dyes removal. Appl. Catal. B 174–175, 445–454. https://doi.org/10.1016/j.apcatb.2015.03.037.

Wang, N., Zhu, L., Huang, Y., She, Y., Yu, Y., Tang, H., 2009a. Drastically enhanced visible-light photocatalytic degradation of colorless aromatic pollutants over TiO_2 via a charge-transfer-complex path: a correlation between chemical structure and degradation rate of the pollutants. J. Catal. 266 (2), 199–206. https://doi.org/10.1016/j.jcat.2009.06.006.

Wang, N., Zhu, L., Wang, M., Wang, D., Tang, H., 2010. Sono-enhanced degradation of dye pollutants with the use of H_2O_2 activated by Fe_3O_4 magnetic nanoparticles as peroxidase mimetic. Ultrason. Sonochem. 17 (1), 78–83. https://doi.org/10.1016/j.ultsonch.2009.06.014.

Wang, Y.-Q., Gu, B., Xu, W.-L., 2009b. Electro-catalytic degradation of phenol on several metal-oxide anodes. J. Hazard. Mater. 162 (2–3), 1159–1164. https://doi.org/10.1016/j.jhazmat.2008.05.164.

Xiang, X., Xie, L., Li, Z., Li, F., 2013. Ternary MgO/ZnO/In_2O_3 heterostructured photocatalysts derived from a layered precursor and visible-light-induced photocatalytic activity. Chem. Eng. J. 221, 222–229. https://doi.org/10.1016/j.cej.2013.02.030.

Xu, W., Fang, J., Chen, Y., Lu, S., Zhou, G., Zhu, X., Fang, Z., 2015. Novel heterostructured Bi_2S_3/$Bi_2Sn_2O_7$ with highly visible light photocatalytic activity for the removal of rhodamine B. Mater. Chem. Phys. 154, 30–37. https://doi.org/10.1016/j.matchemphys.2015.01.040.

Yan, M., Wu, Y., Yan, Y., Yan, X., Zhu, F., Hua, Y., Shi, W., 2016. Synthesis and characterization of novel $BiVO_4$/Ag_3VO_4 heterojunction with enhanced visible-light-driven photocatalytic degradation of dyes. ACS Sustain. Chem. Eng. 4 (3), 757–766. https://doi.org/10.1021/acssuschemeng.5b00690.

Yap, C.L., Gan, S., Ng, H.K., 2011. Fenton based remediation of polycyclic aromatic hydrocarbons-contaminated soils. Chemo-

sphere 83 (11), 1414–1430. https://doi.org/10.1016/j.chemosphere.2011.01.026.

Zhang, G., Lin, B., Yang, W., Jiang, S., Yao, Q., Chen, Y., Gao, B., 2015. Highly efficient photocatalytic hydrogen generation by incorporating CdS into ZnCr-layered double hydroxide interlayer. RSC Adv. 5 (8), 5823–5829. https://doi.org/10.1039/c4ra11757c.

Zhu, S.-R., Qi, Q., Zhao, W.-N., Wu, M.-K., Fang, Y., Tao, K., Yi, F.-Y., Han, L., 2017. Hierarchical core–shell SiO2@PDA@BiOBr microspheres with enhanced visible-light-driven photocatalytic performance. Dalton Trans. 46 (34), 11451–11458. https://doi.org/10.1039/C7DT01581J.